RESEARCH PAPER

Separation of magnetic microparticles in segmented flow using asymmetric splitting regimes

Bert Verbruggen · Tamara Tóth · Matteo Cornaglia · Robert Puers · Martin A. M. Gijs · Jeroen Lammertyn

Abstract A magnetic microparticle-based bioassay requires the separation of the microparticles from the sample matrix, after the microparticles have specifically captured the target of interest. For the implementation of such an assay in water-in-oil droplet segmented flow microfluidics, the particles must be separated from the aqueous sample droplets during a purification step. Current magnetic separation methods pose limits to purification, as only a limited part of the sample volume is removed in the purification step. Combining asymmetric droplet splitting in a T-junction-shaped microfluidic channel with magnetic separation, as induced by a permanent magnet positioned close to the microfluidic channel, is a promising and elegant solution for extracting the magnetic microparticles. However, retaining a high separation efficiency is a challenge and yet untried. In this paper, we describe a microfluidic and magnetic setup to separate superparamagnetic microparticles from the sample droplets, removing up to 90 % of the original sample volume in a single purification step, while keeping the separation efficiency constant. First, the conditions for particle aggregation, attraction and immobilization are determined and used to predict good separation conditions. Second, the magnetic forces at the splitting zone on the microfluidic chip are simulated for different permanent magnet positions and orientations; hereafter, the most promising setups are experimentally realized in polydimethylsiloxane microchannels, tested and the results considering different splitting regimes compared.

Bert Verbruggen and Tamara Tóth have contributed equally to this work.

Electronic supplementary material The online version of this article (doi:10.1007/s10404-014-1409-8) contains supplementary material, which is available to authorized users.

B. Verbruggen · T. Tóth · J. Lammertyn (✉)
BIOSYST-MeBioS, KU Leuven, Willem de Croylaan 42, 3001 Louvain, Belgium
e-mail: jeroen.lammertyn@biw.kuleuven.be

M. Cornaglia · M. A. M. Gijs
Laboratory of Microsystems, Ecole Polytechnique Fédérale de Lausanne (EPFL), Station 17, 1015 Lausanne, Switzerland

R. Puers
ESAT-MICAS, KU Leuven, Kasteelpark Arenberg 10, 3001 Louvain, Belgium

1 Introduction

Lab-on-a-chip technology and micro total analysis systems were introduced in the early nineties of last century and have been growing steadily since then (Manz et al. 1990; Whitesides 2006). One promising and growing subcategory of these microfluidic systems is the field of digital microfluidics (Whitesides 2011). Multiphase, droplet or segmented flow microfluidics use discrete volumes of—mostly—aqueous reagents surrounded by an immiscible fluid or a gas inside microfluidic channels (Günther and Jensen 2006). The confined droplets or plugs have the typical small reaction volumes of a microfluidic system, but prevent cross-contamination between droplets. Transport of the droplets through the microchannels leads to interesting liquid manipulations at a nanoliter scale in a high-throughput context (Anna et al. 2003; Song et al. 2003b). Since the first examples of segmented flow in microfluidic channels, a whole range of applications has been described

in the literature. They deal with the basic droplet operations of formation (Anna et al. 2003; Thorsen et al. 2001), mixing and incubation (Song et al. 2003b), sorting (Baroud et al. 2006; Tang et al. 2009), retention (Huebner et al. 2009), splitting (Link et al. 2004) and merging of droplets (Christopher et al. 2009; Niu et al. 2008). In several applications, the microfluidic operations are combined with heating (Chan et al. 2005) or cooling (Sgro et al. 2007) steps or optical tweezers (He et al. 2005). Most current assays use either on-chip detection with optical techniques or off-chip detection with traditional analytical methods (Song and Ismagilov 2003; Teh et al. 2008).

Many biological applications, such as enzyme linked immunosorbent assays (ELISA) or DNA extraction processes, are often based on magnetic nanoparticles or microparticles as a solid support because of their high surface-to-volume ratio and the potential to magnetically separate them from the sample matrix. Using the magnetic separation allows the removal of unbound and thus unwanted analytes while the immobilized or bound analytes are retained. Magnetic particles have been used in microfluidic systems for some time and several reviews exist on this topic (Gijs et al. 2010; Gijs 2004; Pamme 2006, 2012). The combination of magnetic microparticles with segmented flow is more recent and has been used in immuno-agglutination assays (Teste et al. 2013), for proof-of-principle warfarin detection (Lombardi and Dittrich 2011) and for aspecific DNA extraction (Pan et al. 2011). The splitting and deflecting of ferromagnetic droplets in a magnetic field have been described by AlHetlani et al. (2010).

Current methods of particle separation in segmented flow are based on symmetric droplet splitting (50/50) using a T-junction (AlHetlani et al. 2010; Lombardi and Dittrich 2011). In short, a parent droplet is transported to a split in the channel, the T-junction, where it splits into two identically sized daughter droplets. Before and during the split, a magnet is used to concentrate the magnetic particles to one side of the parent droplet, resulting in a daughter droplet enriched with particles and one depleted of particles. In the ideal case, all particles are contained in one daughter droplet. However, as the droplets are split symmetrically, only half of the original droplet volume is removed and the other half remains with the separated particles. Lab scale and other microfluidic systems can remove up to 99 % in a single step and the separation can be readily repeated to improve the washing the particles. Pan et al. (2011) improved the magnetic separation in segmented flow by splitting the parent droplet slightly asymmetrically. In their system, the daughter droplet containing the magnetic particles consists of only one-third of the original volume. Yet, even by repeating this separation system three times, still 7 % of the unwanted original droplet content remains with the particles. An improved
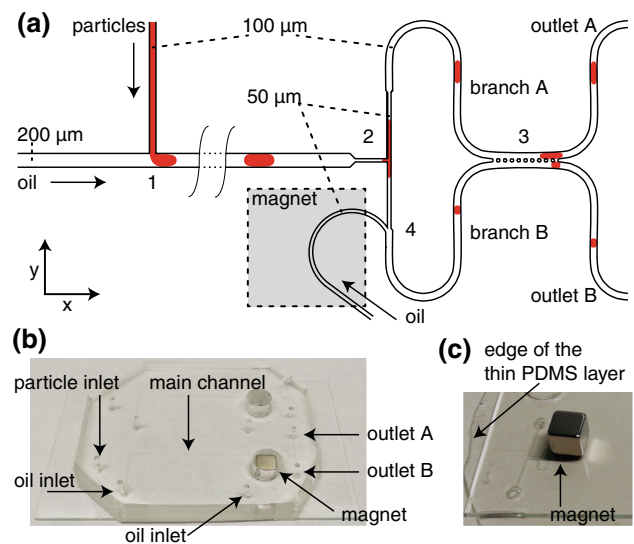

Fig. 1 **a** The final microfluidic design. *1* the droplet formation T-junction, *2* the narrow droplet splitting T-junction, *3* pressure equilibration and *4* extra oil inlet for splitting control. At the T-junction, the main channel splits into two branches called A and B. The magnet location is indicated; however, the exact location was varied throughout the simulations and experiments. **b** A photograph of the actual microfluidic chip, with the magnet embedded in the PDMS. Recognizable features are indicted and a spare channel system currently without a magnet can be seen as well. **c** A close-up of a microfluidic system using the thin PDMS layer. The magnet can be placed anywhere on the thin slab

magnetic separation system is clearly needed to bridge the gap with magnetic separation on continuous microfluidic systems (Lacharme et al. 2009) and EWOD-based digital microfluidic platforms (Ng et al. 2012; Shah 2009; Sista et al. 2008; Wang et al. 2007) and will allow the application of bioassays based on magnetic particle separation.

Recently, we reported on a novel T-junction-based droplet splitting system in which an additional oil flow was applied to dynamically control the droplet splitting ratio. This design is illustrated in Fig. 1. Splitting ratios, defined as the volume of the large daughter droplet over the small daughter droplet, ranging from 50/50 up to 95/5 were achieved without killing the splitting stability (Verbruggen et al. 2013). In a next step, we want to integrate the asymmetric splitting concept with a magnetic particle extraction process. Operational boundaries or optimal conditions of such a process are unknown and experimental trial and error should be avoided as the number of process parameter combinations, including particles type, size, concentrations and microfluidic parameters, is endless. Alternatively, simulation of the hydrodynamic and magnetic forces acting on the particles can guide and reduce the number of experiments. However, hydrodynamic forces on the particles can only be calculated if the flow profile inside a droplet is known. Full three-dimensional models of the flow inside the droplets are computationally very

demanding and have not been reported before. General experimental validation would be challenging, as experimental observations such as the circular flow profile inside a droplet vary considerably between different systems (Dreyfus et al. 2003; Tabeling 2009; Tice et al. 2003). Simulations of the magnetic forces on particles in a continuous flow (Cao et al. 2012; Gassner et al. 2009; Munir et al. 2009; Warnke 2003) and in droplets (Lee et al. 2012) have been described, but for the given purpose, the model should be expanded to include three-dimensional aspects, such as the direction of the forces and the saturation of magnetization of the particles. This will result in a detailed prediction of the forces on any type of particle in any type of microfluidic system.

The main objective of this work was to study the behavior of superparamagnetic microparticles in a magnetic field in segmented flow microfluidics. More specifically, to separate magnetic microparticles into a daughter droplet with a significantly smaller volume compared to current techniques. At the same time, the number of separated particles, the separation efficiency, must remain as high as possible, ideally equal to the equal splitting methods. To achieve this, our previously developed asymmetric splitting concept is used combined with a permanent magnet. First, we use a three-dimensional model of the magnetic flux density and calculate the magnetic forces on three different particle sizes, using the full magnetization curve. Next, keeping all microfluidic parameters constant, the effect of the magnetic force on the particles is experimentally illustrated, and the critical conditions for their aggregation, attraction and immobilization are estimated, both for continuous flow at the sample inlet and for segmented flow in the main channel. Finally, using these boundary conditions, we simulate several practical magnetic setups that involve a permanent magnet as origin for the magnetic field and experimentally compare the most promising separation setups at different asymmetric splitting regimes.

2 Materials and methods

2.1 Reagents and materials

HFE-7500 fluorocarbon oil (3 M, Belgium) was used as continuous phase and 150 mM PBS pH 7.4 containing 0.5 % BSA and 0.01 % Tween 20 as discrete phase. The continuous phase contained 1 % (w/w) of a custom-made polytetrafluoroethylene–polyethyleneglycol block-copolymer surfactant (PFPE–PEG–PFPE) kindly provided by the Weitz lab at Harvard University, USA (Holtze et al. 2008) and had a final viscosity of 0.00124 Pa s and density of 1,614 kg m^{-3}. In this study, three types of superparamagnetic streptavidin-coated microparticles (Dynabeads, Dynal, Norway) with various diameters were used (Table 1). All magnetic microparticles were labeled with biotinylated green fluorescent protein, prepared as described in (Knez et al. 2013) and suspended in the discrete phase.

2.2 Microfluidic device

The microfluidic chip was fabricated in polydimethylsiloxane (PDMS) (Dow Corning, USA) using soft-lithographic techniques (Duffy et al. 1999). In short, SU-8 2050 negative photoresist (Microchem, USA) was spin-coated on a 3 in. wafer at 2,500 RPM and softbaked at 65 and 95 °C. Next, the wafer was exposed to UV light (20 mJ cm^{-2}) through a photomask and baked again at 65 and 95 °C. The unexposed SU-8 was developed and the mold was hard baked in an oven at 95 °C for 1 h. Later, the degassed, liquid PDMS was poured on the mold, spin-coated at 300 RPM and baked at 80 °C, resulting in a 0.5-mm-thick PDMS layer. To shape up the connection for the PEEK tubes, 5-mm-thick pieces of solid PDMS were sealed on top of the thin PDMS layer at the inlets using plasma oxidation. The PDMS film was then peeled from the mold and the inlet and outlet holes were pierced. Finally, the channels were closed by sealing the PDMS to a glass slide and the channels were coated with Aquapel (Pittsburgh Glass Works LLC, USA) to make them strongly hydrophobic.

2.3 Microfluidic design

The microfluidic design used in this work was previously described and allows the dynamic control of the droplet splitting. The splitting ratio, defined as the volume of the large daughter droplet over the small daughter droplet, can be varied from 50/50 to 95/5 (Verbruggen et al. 2013). A schematic representation of the design is reported in Fig. 1. The height of all the channels was 60 μm. It started with

Table 1 Properties of the used Dynabeads, adapted from Fonnum et al. (2005)	Commercial name	Diameter (μm)	Density (g cm^{-1})	Iron content (mg g^{-1})	Maximum magnetization (A m^2 kg^{-1})	Concentration used (mg mL^{-1})
	MyOne streptavidin C1	1.0	1.7	255	24	0.10
	M-280 streptavidin	2.8	1.4	118	10	0.10
	Exosome 4.5 streptavidin	4.4	1.6	202	20	0.35

the droplet formation at the T-junction (1) where a 100 μm side channel joined the main channel (200 μm). At the end the main channel narrowed down to 50 μm and connected to another T-junction, where droplets were split (2). After the split, the two branches (A and B) were broadened back to 100 μm and were partially reconnected to avoid different pressure build up by allowing the oil to flow from one branch to the other through a line of gaps separated by micropillars (3). The droplets continued in their respective channels toward the two outlets and could not pass through the gaps. An additional oil inlet was used to control the splitting ratio (4). Control of the oil flow rate through this oil inlet also permitted control of the total flow rate and pressure in branch B. This in turn allowed steering of the flow rates at the split (2) and thus the asymmetric droplet splitting. When no additional oil was added, the droplets split in two equal daughter droplets. With an additional oil flow, the droplets split asymmetrically, with the smallest daughter droplet going to outlet B and the largest droplet going to outlet A.

2.4 Microfluidic setup

The inlets of the microfluidic chip were connected to glass syringes (Hamilton, Switzerland) by FEB tubes (IDEX, Germany), while PHD 2000 syringe pumps (Harvard Apparatus, USA) were used to precisely control the flow rate in the channels. A 5 mm NdFeB cubic permanent magnet (Supermagnete, Germany) was used to separate the magnetic particles. The chip was mounted on the stage of an inverted fluorescence microscope (IX-71, Olympus, Japan) and the fluorescent signal was captured by the C9100-13 electron multiplier charge-coupled density camera (Hamamatsu, Japan) mounted on the microscope.

2.5 Microfluidic experiments

The continuous flow of suspended particles in the sample inlet channel was kept constant at 0.1 μL min^{-1}. 1 and 2.8 μm particles were used in a concentration of 0.1 mg mL^{-1} and 4.4 μm particles were used in a concentration of 0.35 mg mL^{-1}.

To visualize particle behavior in the main channel with segmented flow, the flow rate of oil and particle suspension was kept constant at 0.4 and 0.1 μL min^{-1}, respectively, to create 30 droplets per minute. Using the same particle concentrations as above, each droplet of 3.33 nL contained on average about 485 particles of 1 μm, 30 particles of 2.8 μm or 25 particles of 4.4 μm. During asymmetric splitting regimes, the control flow rate of oil ranged from 0 to 1.6 μL min^{-1}.

2.6 Numerical simulation of magnetic field density

Finite element method (FEM)-based Comsol Multiphysics 4.2.a (Comsol inc., USA) computational software was used to simulate the 3-D magnetic field imposed by the permanent magnet. A 50-mm cubic air box around the 5-mm cubic magnet proved to be sufficiently large not to force any distortion in the actual magnetic induction distribution. The edge length of the tetrahedron-shaped mesh was varied from 1.5 mm on the outside of the air box to 100 μm at the magnet surface. The relative magnetic permeability of PDMS, glass, oil, water and air was assumed to be 1. In the area of interest, depending on the simulation, a finer mesh with edges of 20 μm was used, to improve the quality of the exported data. Decreasing the mesh size did not change the simulated value of the magnetic force more than 1 %.

While the profile of the magnetic flux density $\mathbf{B}$ (T) can be simulated depending on the geometry, the intensity of $\mathbf{B}$ depends on the magnetization $\mathbf{M}$ (A m^{-1}) of the permanent magnet. The magnetization was determined by measuring $\mathbf{B}$ at various distances from the magnet using a Hall effect sensor and fitting these values with the simulated $\mathbf{B}$ profiles for different magnetization values. The magnetization of the magnet was found to be to 1,400 mT μ_0^{-1} ($R^2 = 0.995$), with μ_0 the permeability of free space. This value was used in the model to simulate both the profile and the intensity of $\mathbf{B}$.

2.7 Calculation of the magnetic forces

The gradient of the magnetic flux density of the permanent magnet and the magnetic force $\mathbf{F_m}$(N) on the paramagnetic microparticles were calculated with Matlab R2010b (MathWorks, USA), using the simulated $\mathbf{B}$ exported from Comsol (grid size 20 μm), as described previously by Cornaglia et al. (2013). The magnetic force acting on a point-like magnetic particle is calculated as (Gijs et al. 2010; Zborowski et al. 1999):

$$\mathbf{F_m} = \frac{1}{\mu_0}(\mathbf{m} \cdot \nabla)\mathbf{B}$$

where $\mathbf{m}$ (A m^2) is the magnetic moment of the superparamagnetic particle. The assumption of a constant magnetic moment is only valid for permanent magnets or in case of a completely saturated magnetization (if $\mathbf{B}$ is large). As in this work superparamagnetic particles were studied in a wide range of $\mathbf{B}$ values, the detailed magnetic properties of the microparticles were obtained from the supplier and the full equation was used to calculate the magnetic force, expanding the range of the model beyond the high field very close to the magnet.
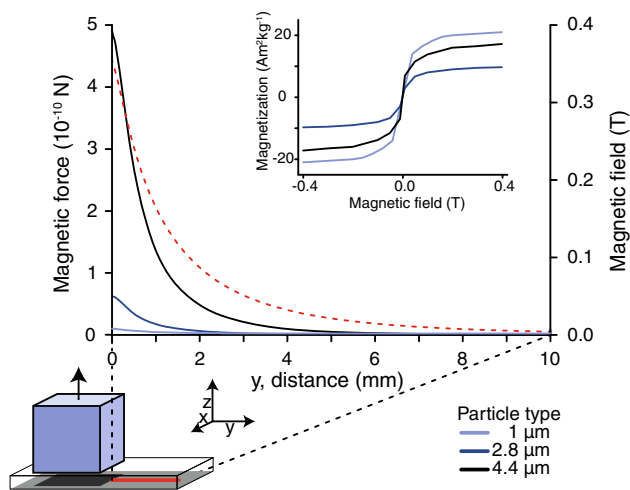
Fig. 2 *Top* the simulated magnetic field (*red dotted line*, *right axis*) as a function of the distance, where $y = 0$ is the edge of the magnet. The magnetic force (*left axis*) on the microparticles depends strongly on their size, 4.4 μm (*black*), 2.8 μm (*dark blue*) and 1 μm particle (*light blue*), but also on the magnetization as a function of the field (*inset*). *Bottom* a schematic representation of the simulated magnetic setup with a Z oriented magnet, indicated by the *arrow*, *on top* of the 0.5 mm PDMS layer, indicated by the *transparent box*. The *red line* represents the location of the cross section used in the graph (color figure online)

3 Results and discussion

3.1 Forces on the superparamagnetic microparticles

The superparamagnetic particles in the microfluidic system are subject to magnetic, hydrodynamic and gravitational forces. Figure 2 shows the simulated **B** (red dotted line, right Y axis) as a function of the distance to the magnet, **B** decreases roughly with the inverse of the cubic distance. The forces calculated at a distance of 0.5 mm below the lower face of the permanent magnet (where later the microfluidic channel will be located) on the three particle types, 4.4 μm (black), 2.8 μm (dark blue) and 1 μm particle (light blue), have a different relation to the distance (left Y axis). Not only the intensity of the magnetic force varies with the distance but also the direction of the force on the microparticles depends on the location (not shown). The inset clearly illustrates that the mass magnetization in function of **B** cannot be simplified to a linear increase or a constant value. Note that the maximum magnetization is not related to the particle size, but to the fraction of iron oxide they contain (Fonnum et al. 2005).

Superparamagnetic particles in a magnetic field attract each other spontaneously forming aggregates. While the magnetic force of the aggregate is equal to the sum of the individual particles, the drag force on the aggregate is lower than the sum of the individual drag forces. Thus, the formation of large aggregates is beneficial for the manipulation of the magnetic particles in a flow. The size of the

aggregate is determined by the magnetic field, the magnetization of the particles and the hydrodynamic forces breaking them up. If the magnetic force on particles or aggregates is sufficiently large, the particles can become immobile against the channel wall and cause the droplet to break, leaving a small water layer around the particles.

The magnetic particles also undergo hydrodynamic forces in the continuous and discrete flow regime. A continuous flow inside a microfluidic channel has a typical parabolic profile, with the liquid moving fast in the center and slower at the channel walls. In segmented flow microfluidics, circular flow profiles are observed in the droplets (Song et al. 2003a), with the flow properties depending on several parameters including the liquid composition and properties, the surfactants and the channel dimensions. In this particular system, the oil pulls the droplets through the channels, as some oil continuously slips past the droplet, pulling the outer fluid layers of the droplet forward. The detailed flow modeling falls outside the scope of this work, as it would be complex, computationally intensive and hard to validate experimentally. The aggregation of the particles would further complicate accurate calculations.

The force on the microparticles due to gravity and the final sedimentation velocity are calculated using diameter and density values provided by the supplier. Corrected for buoyancy, the calculated force is equal to 4.1×10^{-15}, 4.7×10^{-14} and 2.6×10^{-13} N, and the sedimentation velocity is thus approximately 4.2×10^{-7}, 1.6×10^{-6} and 6.3×10^{-6} m s^{-1} for the 1.0, 2.8 and 4.4 μm particles, respectively. While gravitation cannot be neglected, it is hard to visualize as vertical movement of the particles cannot be visualized from below with the inverted microscope. Some settling particles are observed in most experiments, but they are actively re-suspended by the hydrodynamic forces.

3.2 Particle behavior in a magnetic field

3.2.1 Particle behavior in a magnetic field: continuous flow

Initially, before the droplets are formed, the microparticles are transported to the main channels through the inlet channel in a continuous flow. The particle suspension should be homogenously distributed in the inlet channel to minimize variation of the particle concentration in the droplets. Any magnetic force working on the particles influences the distribution of the particles and must thus be avoided.

The behavior of the magnetic particles inside the continuous flow of the sample inlet was studied as a function of the magnet-channel distance. All droplets were imaged
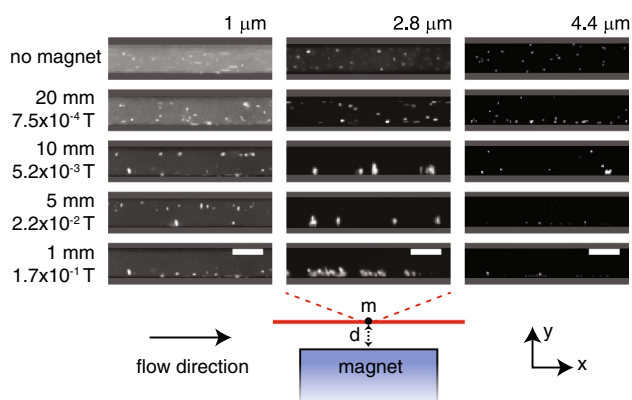
Fig. 3 *Top* top view of the inlet channel with a continuous flow, showing the behavior of the superparamagnetic particles, before the droplet formation. Decreasing the distance (d) between the channel and the magnet increases the magnetic field and thus the magnetic force. The three particle types are presented side by side: 1 and 2.8 μm particles were used in a concentration of 0.1 mg mL^{-1} and 4.4 μm particles were used in a concentration of 0.35 mg mL^{-1}. The 4.4 μm particles tend to move both toward the side and the bottom of the channel, hereby concentrating below the optimal focal point of the microscope. This makes the particles less intense and appear less numerous. The *scale bar* represents 100 μm. *Bottom* a schematic representation of the simulated magnetic setup, a Z oriented magnet *on top* of the 0.5 mm PDMS layer. The *red line* represents the channel, with point m the center of the magnet and the location of the images and d the distance between point m and the magnet (color figure online)
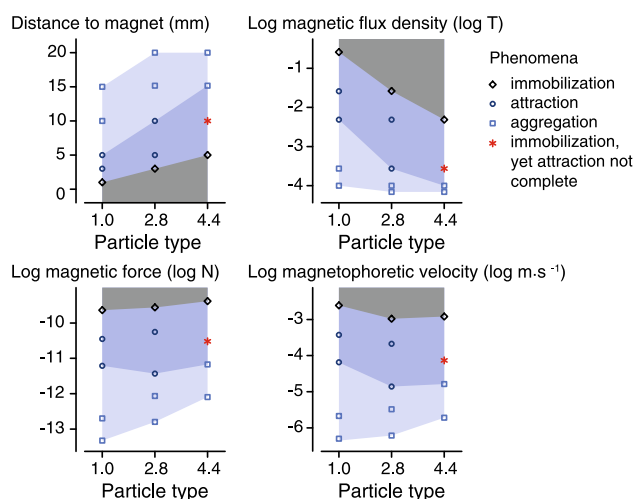

Fig. 4 The magnetic phenomena visible in the continuous flow for the three different particle types (1, 2.8 and 4.4 μm): complete aggregation of the particles (*light blue*), complete attraction toward the channel wall (*blue*) and complete immobilization against the channel wall (*dark gray*). The distance between the channel and the magnet, the maximal intensity of B, the magnetic force acting on the microparticles and the resulting magnetophoretic velocity are related parameters and are used to visualize the boundaries conditions at which the magnetic phenomena occur. In case of the 4.4 μm particle, a different behavior was seen at about 10 mm, where the microparticles were immobilized against both the bottom and the side wall of the channel (*red star symbol*) (color figure online)

at the middle of the magnet edge (point m), where the magnetic force parallel to the channel ($\mathbf{F_x}$) was zero. Figure 3 illustrates the behavior of the three particle types in the case of a Z oriented magnet at a variable distance (i.e., a magnet with the magnetization orientation along the Z axis) and placed aside the microfluidic channel. Without a magnet, the particles move freely from left to right, with a higher velocity in the center due to the typical parabolic flow profile in continuous flow. In the presence of a magnet, three phenomena were distinguished: aggregation, attraction and immobilization of the magnetic particles. Aggregation is defined by the formation of microparticle aggregates and is considered complete when no individual microparticles remain. At the same time, attraction toward the magnet occurs and results in particle transport toward the channel wall. This is considered complete when the aggregates are moving parallel to the channel, close to the channel wall. If the magnet is moved even closer to the channel, the aggregates stop moving completely and are immobilized again the wall.

Figure 4 shows the parameter values at which the microparticles were completely aggregated, attracted against the channel wall or immobilized, for the three particle types. The represented parameters are the distance (d) between the magnet and the channel, the intensity of **B** in the channel, the magnetic force acting on the microparticles ($\mathbf{F_m}$) and the resulting magnetophoretic velocity

($\mathbf{V_m}$), which is the equilibrium velocity for which the magnetic and drag force are equal. While the parameters are closely related, the differences between the graphs illustrate some observations.

At $\mathbf{V_m}$ around 10^{-6} m s^{-1}, all microparticles were completely aggregated, and thus, the order of magnitude of the $\mathbf{V_m}$ appears a better predictor than the distance or the order of magnitude of $\mathbf{F_m}$, which varied more between the particle types. $\mathbf{V_m}$ does indeed take both $\mathbf{F_m}$ and particle size into account. It can be noted that the $\mathbf{V_m}$ here was much lower than the average flow velocity of the fluid, which was about 2.8×10^{-4} m s^{-1}. The complete attraction of the particles toward the magnet, when they move along the channel wall, was reached for $\mathbf{F_m}$ between 10^{-11} and 10^{-12} N where $\mathbf{V_m}$ was between 10^{-4} and 10^{-5} m s^{-1}. The largest particles (4.4 μm) had a point where all microparticles were immobilized again both the bottom and the side wall of the channel (Fig. 3, at 10 mm). This is indicated in Fig. 4 with a red star. Complete immobilization against the channel wall closest to the magnet was seen for $\mathbf{F_m}$ above 10^{-10} N or $\mathbf{V_m}$ above 10^{-3} m s^{-1} for all three microparticles types.

It is clear from these results that $\mathbf{F_m}$ on a particle or $\mathbf{V_m}$ of the particle at which the phenomena occurred, corresponded well between different particles and thus appeared to be good prediction parameters. On the other hand, the
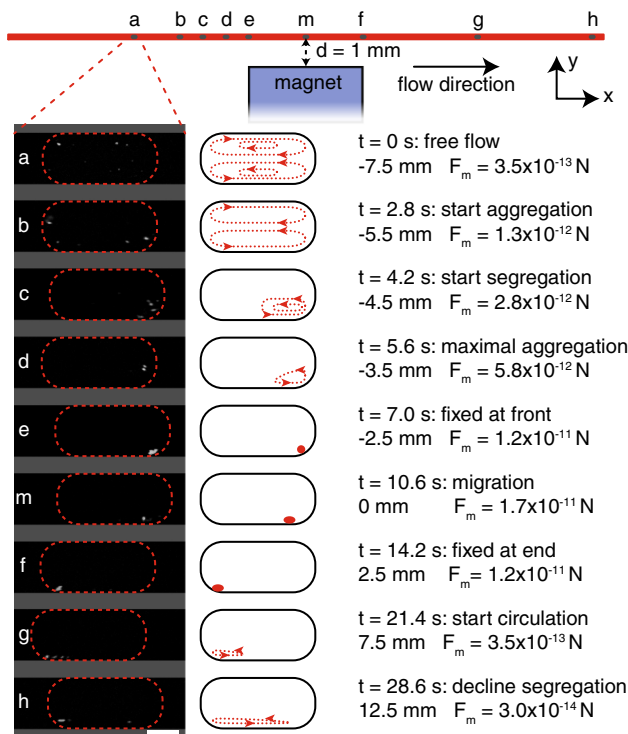
Fig. 5 Top view of the main channel, showing the particle behavior in a droplet while passing aside the magnet in the main microfluidic channel. The illustrations show the visually observed path of the particles at this location. The 2.8 μm particles initially aggregate and move to the front of the droplet (**a–d**), overcoming hydrodynamic forces. Next, a solid clump is formed that moves from the front to the back of the droplet as the magnet is passed (**e**, **f**). Finally, the clump starts to bounce from back to front and breaks into smaller aggregates (**f–h**). These aggregates remain long after the magnet is passed. The *scale bar* represents 100 μm. The magnetic setup is identical to the previous experiments, represented the *bottom panel* of Fig. 3

distance to the magnet and thus also the intensity of **B** could not be used to predict the three phenomena. This confirmed the importance of calculating the actual magnetic forces, instead of merely modeling B. The results of this experiment were directly used when designing the final microfluidic system, as the minimal distance between the sample inlet and the magnet to avoid aggregation, attraction to the side or immobilization could now be estimated for different types of particles. To avoid attraction to the channel wall and the formation of aggregates in this particular system, the minimum distance between the magnet and the sample inlet channel (Fig. 1a, point 1) was 10 mm for 1 μm particles and at least 20 mm was necessary for 2.8 and 4.4 μm particles.

3.2.2 Particle behavior in a magnetic field: segmented flow

To study the behavior of magnetic microparticles inside the droplets in a magnetic field, two separate experiments were performed. The droplets were first imaged at different locations along the main channel passing the magnet, to visualize the particle behavior while entering and leaving the magnetic field. In a second experiment, the magnet-channel distance was varied and droplets were imaged when passing the middle of the magnet edge at point m where F_x was zero. This allowed determining the conditions needed for particle aggregation or immobilization. In order to limit the number of measurements, the flow rate was kept constant, thus keeping the maximum and average hydrodynamic forces acting on the particles constant as well.

3.2.2.1 Evolution while passing the magnet In the first experiment, the distance between the magnet and the main channel (d) was kept constant at 1 mm and the droplets were imaged at various locations along the channel (Fig. 5). In these locations, the magnetic force was not always perpendicular to the channel and the final location of the particles was thus not always in the front of the droplet. Only the results of the 2.8 particles are discussed here, but the 1 and 4.4 μm particles show the same type of behavior.

At the T-junction with the main channel, the magnetic particle suspension was split in droplets, enclosed by the carrier oil. The average flow velocity in the microfluidic channel was 7.0×10^{-4} m s^{-1}, but inside the droplet, the flow profile was not the parabolic profile of continuous flow, but a closed circular flow (Song et al. 2003a). Without a magnet next to the channel, the particles moved rapidly forward at the droplet edge and returned slowly backward through the center of the droplet (Fig. 5, point a). With a magnet present, a magnetic force acts on the microparticles causing acceleration of the microparticles toward the highest **B** (visible from point b and further). This acceleration was counteracted by the drag force, resulting in a constant velocity relatively to the velocity of the circulation flow profile: the magnetophoretic velocity (V_m).

At point a (7.5 mm before point m), the magnetic force was still very weak. Particles swirl around in the drop, as demonstrated by the cartoon, actually visualizing the flow profile inside the droplet. Between point b–e (5.5–2.5 mm before point m), the particles aggregated and were attracted toward the magnet. This also brought the particles forward into the droplet and the circulation of the particles gradually reduced to a small area in the front of the droplet, close to the channel wall in the direction of the magnet (point e). The clump of particles remained at this position inside the droplet till point m, where the magnetic force started pulling the particles to the back of the droplet, against the local direction of the circulating flow. As the droplets passed the right edge of the magnet, at point f, the magnetic
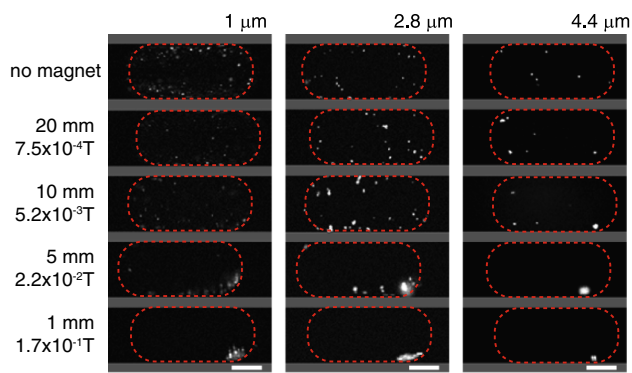
Fig. 6 Top view of a segmented flow in the main channel at point m, showing the behavior of particles. Decreasing the distance (d) between the channel and the magnet increases the magnetic field and thus the magnetic force. The three particle types are presented side by side. The *scale bar* represents 100 μm. The magnetic setup is identical to the setup presented in the *bottom panel* of Fig. 3

Fig. 7 The magnetic phenomena visible in the droplets for the three different particle types (1, 2.8 and 4.4 μm): complete aggregation of the particles (*light blue*), complete attraction toward the channel wall (*blue*) and complete immobilization against the channel wall (*dark gray*). The distance between the channel and the magnet, the maximal intensity of **B**, the magnetic force acting on the microparticles and the resulting magnetophoretic velocity are related parameters and are used to visualize the boundaries conditions at which the magnetic phenomena occur. Higher values are needed in segmented flow to observe all three phenomena compared with continuous flow (color figure online)

force dropped below 5×10^{-13} N and the particles started to swirl around in a small zone in the droplet. After point h, 12.5 mm beyond point m, the clump was broken into smaller aggregates and the particles started to circulate again, but remained close to the channel wall and the magnet. The single compact aggregate of particles, confined to one side of the droplet, should lead to better microparticle separation, and therefore, the T-junction split should be close to and in no case further than 12.5 mm from the center of the magnet.

It is clear that the particle behavior was not symmetric with respect to the magnet. Once the aggregate was formed, the particles remain aggregated even at lower magnetic forces. After passing the magnet, the aggregate was also confined to one side of the droplet due to the intra-droplet hydrodynamic forces. The complete re-suspension and homogeneous dispersion of the particles required a turbulent force and/or more time. The behavior of the particles with and without magnetic field is also demonstrated in supplementary video 1 and 2.

3.2.2.2 Influence of the maximal magnetic field In this experiment, the magnetic forces were varied by changing the distance d between magnet and channel. As these images were taken at point m, the magnetic force along the channel (F_x) was zero. Figure 6 presents the observed behavior of the three particles types inside the droplets at four magnet-channel distances (d). The three phenomena, aggregation, attraction and immobilization, could be distinguished as well in the segmented flow. While aggregation was very similar to the continuous flow, the other two phenomena differed between the continuous and segmented flow. First, movement toward the magnet brought the particles into a zone with higher forward flow velocity,
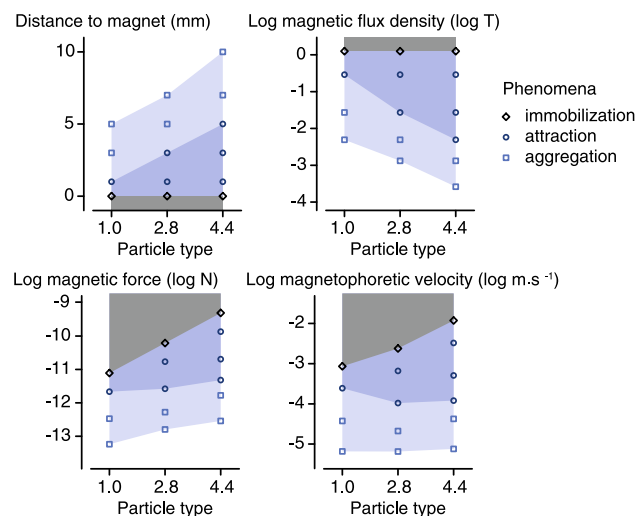
and thus, the particles moved to the front of the droplet. Secondly, as the droplet meniscus kept the particles in the droplet, they remain mobile at much higher magnetic forces. When the particles eventually were immobilized, the droplet broke as a small part of the droplet volume remained behind with the particles.

Figure 7 illustrates the critical conditions for the three phenomena. The complete particle aggregation in the drops required a minimal distance of 5 mm for both the 1 and the 2.8 μm particles, while the larger 4.4 μm particles exhibited already complete aggregation at 10 mm distance. F_m appears a better parameter to predict the complete aggregation of microparticles in segmented flow, in the order of 10^{-13} N. This is two orders of magnitude higher compared with continuous flow, which is thought to be due to the intra-droplet circulation flow profile. V_m was about 7×10^{-6} m s^{-1} and is thereby the best parameter to predict the complete aggregation.

The F_m values whereby the three particles types were completely attracted to the edge of the droplet were around 3×10^{-12}, again significantly higher compared with completed attraction in continuous flow. The calculated V_m here was about 10^{-4} m s^{-1} and can be used to predict the complete attraction as well, whereas the distance or the order of magnitude of **B** cannot. If the magnetic force was increased further, the particles were retained at the channel wall while the drop traveled onward. On the one hand, the

intensity of **B** necessary to immobilize the small particles was much higher than that needed to immobilize the larger particles. On the other hand, the magnetic force acting on the small particles was lower (3.0×10^{-12} N) than the force needed to immobilize the large particles (2.4×10^{-11} and 4.9×10^{-10} N). These forces could only be reached at the edge of or directly under the magnet, thus in order to avoid immobilization, the magnet should not be on top of the channel.

3.3 Magnet position and orientation at the split

As shown by other authors (Lee et al. 2012; Lombardi and Dittrich 2011; Pan et al. 2011), splitting a droplet while attracting the magnetic particles can be used to separate the particles into one daughter droplet. During the split, the internal flow profiles are very complex and single particles often end up in both daughter droplets and are thus not completely separated. It is expected that attempting to separate particles into increasingly smaller daughter droplets might lead to a higher number of particles flowing into the wrong droplet. On the one hand, the magnetic forces must be sufficiently high to keep the particles grouped in one compact aggregate (minimally 10^{-12} N) and to pull this clump into the correct daughter droplet (maximum F_Y). On the other hand, the external magnet cannot be too close to any part of the channel such that particles are immobilized and pulled out of the droplets. To avoid this completely, the magnetic force should remain well below 10^{-12}, 10^{-11} and 10^{-10} N anywhere in the channels, for, respectively, the 1, 2.8 and 4.4 μm particles.

Using the microfluidic setup described in the materials and methods section (Fig. 1), the magnet was introduced. The magnet was either positioned on top of the glass (Fig. 6b) or embedded in the PDMS (c). In the latter case, the magnet and channels were separated by 1 mm of PDMS to avoid leakage. Alternatively, the magnet was positioned on top of a thin 0.5 mm PDMS layer to avoid the risk of leakage between the magnet and the channel. Moving the magnet 0.5 mm upward significantly lowered **B** in the channels close to the magnet, but the ability to position the magnet closer to the split, on top of the control channel without leakage, in turn increased **B** locally. Within these two configurations, the direction of the magnetization of the magnet was oriented in the *X*, *Y* and *Z* directions and placed at different angles with respect to the splitting T-junction itself. The magnetic force at the split (point s) was divided into the *X*, *Y* and *Z* components and the results of the most promising configurations are summarized in Fig. 8 (other data not shown).

Using the 2.8 μm particles, the maximum force of 2.4×10^{-11} N was only reached at the edge of the magnet. A safe distance of 1 mm between the magnet edge and the
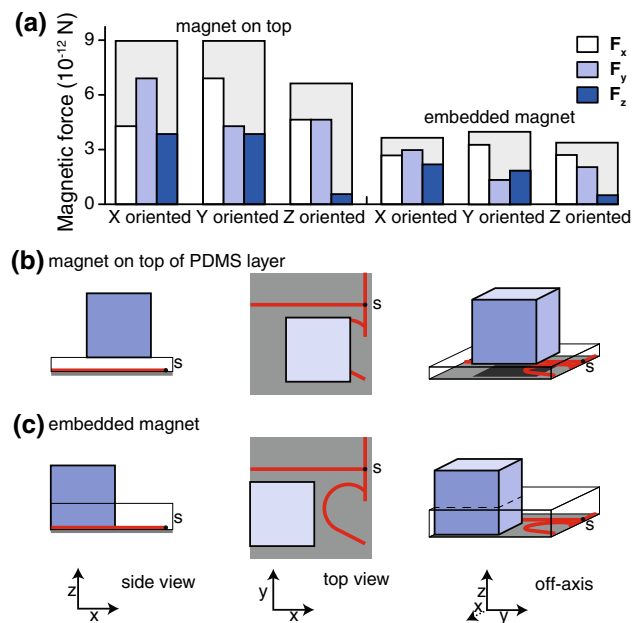

Fig. 8 a The absolute values of the three components of the magnetic force on 2.8 μm particles for 6 positions at point s: *white* for F_x, *light blue* for F_y and *dark blue* for F_z. The total magnetic force is shown in *gray*. **b** The configurations of the magnet, on top of the thin PDMS layer (*transparent box*). **c** The magnet embedded in the PDMS (*transparent box*), in contact with the glass (color figure online)

center of the channel was chosen, as a smaller distance could not be achieved accurately without micromanipulators to position the magnet accurately. Even with this additional safe distance, the three configurations on top of the PDMS layer resulted in a higher total magnetic force at the splitting zone. The increased height of the magnet was clearly compensated by the decreased distance from the splitting zone. Both the *X* and *Y* oriented magnets on top had a higher total magnetic force, compared with the *Z* oriented magnet and thus performed better to separate particles. The *X* oriented magnet had an additional benefit of having a high F_Y component, pulling the particles strongly in the preferred daughter droplet. However, both *X* and *Y* oriented magnet configurations appeared to have a high F_Z, attracting the particle aggregates in the *Z* direction almost as much as toward the correct side of the splitting zone.

In case of a *Z* oriented magnet, the total force (6.6×10^{-12} N) was still well above the critical threshold of about 7×10^{-13} N needed to complete the aggregation of this type of particles (Fig. 7). This results in a single aggregate arriving at the split. The components of the force in the *Z* direction were rather small and the direction of the total force was favorable to the other two situations. The F_X was probably less important as it was aligned with the average flow inside the droplet and thus only influenced the velocity of the backward or forward migration of aggregates inside the droplet.
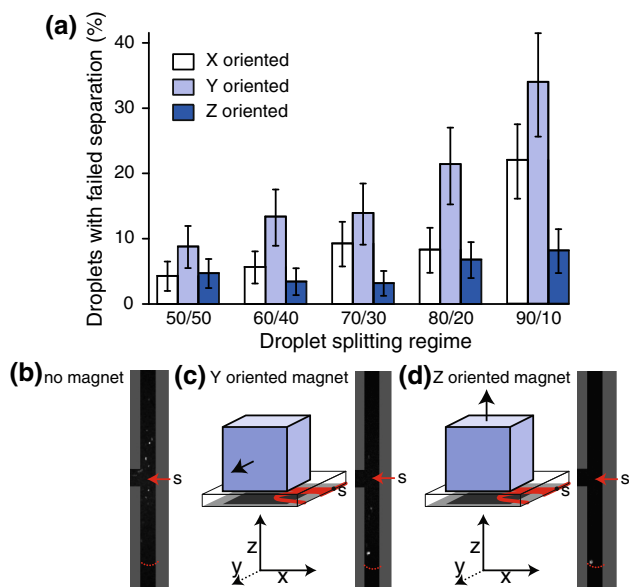
Fig. 9 Experimental separation results at different splitting regimes. **a** The percentage of droplets with failed separation, counted by analyzing 80–120 droplets. The *X* oriented (*white*) and *Y* oriented (*light blue*) setup failed increasingly at more asymmetric splitting regimes, while the *Z* oriented magnet (*dark blue*) had a near constant and low failure rate. The *error bars* represent one standard deviation. **b** A typical image of splitting without magnet. **c** Splitting with a *Y* oriented magnet. **d** Splitting with a *Z* oriented magnet. The *red dotted line* indicates the droplet edge of the forming daughter droplet. The channels are 50 μm wide at the splitting T-junction (color figure online)

The configurations with the magnet on top of the thin PDMS layer (Fig. 8b) appeared promising for successful microparticle separation for using either a *X*, *Y* or *Z* oriented magnetization. Therefore, the magnetic separation was tested in these three cases at different splitting regimes. Equal splitting (50/50) was achieved without an additional oil flow through the control channel, while the asymmetric splitting regimes required an increasing control flow, up to 1.6 μL min^{-1}. In the most asymmetric droplet splitting regime (90/10), one daughter droplet contained 10 % and the other 90 % of the original volume of the parent droplet. As the exact number of particles in each daughter droplet was hard to determine, a failed separation was defined as a separation where at least one particle or aggregate was not correctly separated during a droplet split. By this stringent definition, all separations failed in case of the 1 μm particles, as some particles always remained in the larger daughter droplet. The largest microparticles (4.4 μm) were nearly always completely separated, with only an occasional particle in the wrong daughter droplet. Both cases make it hard to determine the best magnet configuration.

The 2.8 μm particles were more interesting, as the number of failed separations clearly depended on the location and orientation of the magnet. By analyzing between 80 and 120 daughter droplets at outlet A for each

magnet configuration and splitting regime, the failure rate of the separation was determined (Fig. 9).

In general, the separation efficiency decreased when the asymmetry of the splitting regime was increased. This can be readily explained, as it becomes increasingly hard to collect all microparticles in the decreasing volume of the daughter droplet. It is also clear from the results that the *Y* oriented magnet setup had the highest failure rate for every splitting regime and that the failure rate increased with increasing asymmetric split. The *Z* oriented setup on the other hand, with a lower total magnetic force and about the same F_Y, separated best at any regime and the separation efficiency remained approximately constant. The *Z* oriented setup is thus clearly the best choice for magnetic microparticle separation in this system. The *X* oriented setup performed intermediate, even though it had the highest F_Y of all. The F_Y at the split was clearly not the only parameter determining a good separation.

When comparing images taken during the actual split, the *Z* oriented setup mostly contained a single aggregate (Fig. 9, point d), while the other two setups tended to have multiple smaller aggregates (c). Smaller aggregates were subjected to both smaller magnetic and hydrodynamic forces and the magnetic force on an aggregate was linearly proportional on the number of particles. The hydrodynamic force depended on the radius of the aggregates and declined slower with decreasing number of particles in the aggregate. Smaller aggregates were thus comparably more subjected to the hydrodynamic force, explaining the higher failure rate. While this partial breakup can explain the difference in separation performance, its origin is harder to find. In all three situations, the particles form a single aggregate and this aggregate remains intact at least until passing the edge of the magnet. Thus, all three situations appear to enter the splitting and separation zone with the same starting conditions. It is speculated that the higher F_Z of the *X* and *Y* oriented magnets caused the aggregates to move toward the ceiling of the channel. The combination of a high flow velocity at the edge of the droplet and the F_Z caused the aggregate to bump against the PDMS repeatedly, thus causing the breakup.

4 Conclusion

In this work, a detailed three-dimensional model of the magnetic field in proximity of a cubic permanent magnet was used to accurately calculate the magnetic force on superparamagnetic particles. Hereby, the complete magnetization curve of the particles was used, increasing the working range of the model beyond the very high magnetic flux density conditions. This model was first applied to study particle behavior in continuous flow what resulted in

an estimation of the minimum distance between the particle inlet and magnet depending on the particle type.

Secondly, droplets with particles were followed while passing the magnet to study the gradual aggregation and attraction toward the magnet. The single aggregate, formed while passing the magnet, started to break into smaller parts when the magnetic force dropped below 10^{-12} N. This should be avoided to improve separation. Thirdly, particle aggregation, attraction and movement toward the magnet and complete immobilization in droplets were described using accurate magnetic forces, force components or magnetophoretic velocities. To achieve complete particle aggregation, the magnet had to be close enough to the channel to induce a $\mathbf{V_m}$ of about 10^{-5} m s^{-1}. The aggregates joined together in one single aggregate around $\mathbf{F_m} = 10^{-11}$ N. The attraction toward the magnet improved with increasing $\mathbf{F_Y}$ conditions, but to avoid immobilization of the aggregates, the total magnetic force had to remain below a maximum magnetic force.

Following, the model was used to simulate several practical configurations for particle separation during droplet splitting whereby the best setup was now selected based on the actual size and direction of the magnetic force at the split. Positioning the magnets closer to the actually split location, even if the magnet cannot be placed against the glass but must be on a 0.5 mm layer of PDMS, gave the highest forces, regardless of magnet orientation. Both the Z oriented and the Y oriented magnet situations appeared to have advantages and were used in experiments in combination with different splitting regimes, ranging from 50/50 to 90/10. These results demonstrate the superiority of the Z oriented magnet, especially in the more asymmetric splitting regimes, probably due to a compact single aggregate. With this setup, the objective of this paper was reached, as the microparticles can be separated into a daughter droplet of 10 % of the volume of the parent droplet, without a significant change of the separation efficiency. This is an important step forward compared with the (near) equal splitting used in previously reported separation concepts.

Future research should include additional simulations and experiments to study the influence of the hydrodynamic forces, as well as the particle concentration and aggregation, in order to get a more complete understanding of magnetic particle manipulation in droplets. The magnetic setup developed in this paper might be improved using more precise methods to place the magnet closer to the split.

References

AlHetlani E, Hatt O, Vojtíšek M, et al (2010) Magnetic droplets–generation and manipulation in continuous flow. In: Proceedings of the 14th International Conference on Miniaturized Systems for Chemistry and Life Sciences. Groningen, The Netherlands, pp 1817–1819. http://www.rsc.org/binaries/LOC/2010/PDFs/Papers/619_0892.pdf

Anna SL, Bontoux N, Stone HA (2003) Formation of dispersions using "flow focusing" in microchannels. Appl Phys Lett 82:364. doi:10.1063/1.1537519

Baroud CN, Delville J-P, Gallaire F, Wunenburger R (2006) Thermocapillary valve for droplet production and sorting. Phys Rev E Stat Nonlinear Soft Matter Phys 75:046302

Cao Q, Han X, Li L (2012) Numerical analysis of magnetic nanoparticle transport in microfluidic systems under the influence of permanent magnets. J Phys D Appl Phys 45:465001. doi:10.1088/0022-3727/45/46/465001

Chan EM, Alivisatos AP, Mathies RA (2005) High-temperature microfluidic synthesis of CdSe nanocrystals in nanoliter droplets. J Am Chem Soc 127:13854–13861. doi:10.1021/ja051381p

Christopher GF, Bergstein J, End NB et al (2009) Coalescence and splitting of confined droplets at microfluidic junctions. Lab Chip 9:1102–1109. doi:10.1039/b813062k

Cornaglia M, Tekin HC, Lehnert T, Gijs MAM (2013) Fine-tuning of magnetic and microfluidic viscous forces for specific magnetic bead-based immunocomplex formation. J Appl Phys 114:064903. doi:10.1063/1.4817663

Dreyfus R, Tabeling P, Willaime H (2003) Ordered and disordered patterns in two-phase flows in microchannels. Phys Rev Lett 90:1–4. doi:10.1103/PhysRevLett.90.144505

Duffy DC, Schueller OJA, Brittain ST, Whitesides GMG (1999) Rapid prototyping of microfluidic switches in poly(dimethyl siloxane) and their actuation by electro-osmotic flow. J Micromech Microeng 9:211–217

Fonnum G, Johansson C, Molteberg A et al (2005) Characterisation of Dynabeads® by magnetization measurements and Mössbauer spectroscopy. J Magn Magn Mater 293:41–47. doi:10.1016/j.jmmm.2005.01.041

Gassner A-L, Abonnenc M, Chen H-X et al (2009) Magnetic forces produced by rectangular permanent magnets in static microsystems. Lab Chip 9:2356–2363. doi:10.1039/b901865d

Gijs MAM (2004) Magnetic bead handling on-chip: new opportunities for analytical applications. Microfluid Nanofluidics 1:22–40. doi:10.1007/s10404-004-0010-y

Gijs MAM, Lacharme F, Lehmann U (2010) Microfluidic applications of magnetic particles for biological analysis and catalysis. Chem Rev 110:1518–1563. doi:10.1021/cr9001929

Günther A, Jensen KF (2006) Multiphase microfluidics: from flow characteristics to chemical and materials synthesis. Lab Chip 6:1487–1503. doi:10.1039/b609851g

He M, Edgar JS, Jeffries GDM et al (2005) Selective encapsulation of single cells and subcellular organelles into picoliter- and femtoliter-volume droplets. Anal Chem 77:1539–1544. doi:10.1021/ac0480850

Holtze C, Rowat AC, Agresti JJ et al (2008) Biocompatible surfactants for water-in-fluorocarbon emulsions. Lab Chip 8:1632–1639. doi:10.1039/b806706f

Huebner A, Bratton D, Whyte G et al (2009) Static microdroplet arrays: a microfluidic device for droplet trapping, incubation and release for enzymatic and cell-based assays. Lab Chip 9:692–698. doi:10.1039/b813709a

Knez K, Noppe W, Geukens N et al (2013) Affinity comparison of p3 and p8 peptide displaying bacteriophages using surface plasmon resonance. Anal Chem 85:10075–10082. doi:10.1021/ac402192k

Lacharme F, Vandevyver C, Gijs MAM (2009) Magnetic beads retention device for sandwich immunoassay: comparison of off-chip and on-chip antibody incubation. Microfluid Nanofluidics 7:479–487. doi:10.1007/s10404-009-0424-7

Lee H, Xu L, Ahn B et al (2012) Continuous-flow in-droplet magnetic particle separation in a droplet-based microfluidic platform. Microfluid Nanofluidics 13:613–623. doi:10.1007/s10404-012-0978-7

Link DR, Anna S, Weitz DA, Stone HA (2004) Geometrically mediated breakup of drops in microfluidic devices. Phys Rev Lett 92:054503. doi:10.1103/PhysRevLett.92.054503

Lombardi D, Dittrich PS (2011) Droplet microfluidics with magnetic beads: a new tool to investigate drug-protein interactions. Anal Bioanal Chem 399:347–352. doi:10.1007/s00216-010-4302-7

Manz A, Graber N, Widmer HM (1990) Miniaturized total chemical analysis systems: a novel concept for chemical sensing. Sens Actuators B Chem 1:244–248. doi:10.1016/0925-4005(90)80209-I

Munir A, Wang J, Zhou HS (2009) Dynamics of capturing process of multiple magnetic nanoparticles in a flow through microfluidic bioseparation system. IET Nanobiotechnol 3:55–64. doi:10.1049/iet-nbt.2008.0015

Ng AHC, Choi K, Luoma RP et al (2012) Digital microfluidic magnetic separation for particle-based immunoassays. Anal Chem 84:8805–8812. doi:10.1021/ac3020627

Niu X, Gulati S, Edel JB, DeMello AJ (2008) Pillar-induced droplet merging in microfluidic circuits. Lab Chip 8:1837–1841. doi:10.1039/b813325e

Pamme N (2006) Magnetism and microfluidics. Lab Chip 6:24–38. doi:10.1039/b513005k

Pamme N (2012) On-chip bioanalysis with magnetic particles. Curr Opin Chem Biol 16:436–443. doi:10.1016/j.cbpa.2012.05.181

Pan X, Zeng S, Zhang Q et al (2011) Sequential microfluidic droplet processing for rapid DNA extraction. Electrophoresis 32:1–7. doi:10.1002/elps.201100078

Sgro AE, Allen PB, Chiu DT (2007) Thermoelectric manipulation of aqueous droplets in microfluidic devices. Anal Chem 79:4845–4851. doi:10.1021/ac062458a

Shah GJ (2009) Meniscus-assisted high-efficiency magnetic collection and separation for EWOD droplet microfluidics. J Microelectromech Syst 18:363–375. doi:10.1109/JMEMS.2009.2013394

Sista RS, Eckhardt AE, Srinivasan V et al (2008) Heterogeneous immunoassays using magnetic beads on a digital microfluidic platform. Lab Chip 8:2188–2196. doi:10.1039/b807855f

Song H, Ismagilov RF (2003) Millisecond kinetics on a microfluidic chip using nanoliters of reagents. J Am Chem Soc 125:14613–14619. doi:10.1021/ja0354566

Song H, Bringer MR, Tice JD et al (2003a) Experimental test of scaling of mixing by chaotic advection in droplets moving through microfluidic channels. Appl Phys Lett 83:4664–4666. doi:10.1063/1.1630378

Song H, Tice JD, Ismagilov RF (2003b) A microfluidic system for controlling reaction networks in time. Angew Chemie 115:792–796. doi:10.1002/ange.200390172

Tabeling P (2009) A brief introduction to slippage, droplets and mixing in microfluidic systems. Lab Chip 9:2428–2436

Tang SKY, Li Z, Abate A et al (2009) A multi-color fast-switching microfluidic droplet dye laser. Lab Chip 9:2767–2771. doi:10.1039/b914066b

Teh S-Y, Lin R, Hung L-H, Lee AP (2008) Droplet microfluidics. Lab Chip 8:198–220. doi:10.1039/b715524g

Teste B, Ali-Cherif A, Viovy J-LL, Malaquin L (2013) A low cost and high throughput magnetic bead-based immuno-agglutination assay in confined droplets. Lab Chip 13:2344–2349. doi:10.1039/c3lc50353d

Thorsen T, Roberts RW, Arnold FH, Quake SR (2001) Dynamic pattern formation in a vesicle-generating microfluidic device. Phys Rev Lett 86:4163–4166. doi:10.1103/PhysRevLett.86.4163

Tice JD, Song H, Lyon AD, Ismagilov RF (2003) Formation of droplets and mixing in multiphase microfluidics at low values of the Reynolds and the capillary numbers. Langmuir 19:9127–9133. doi:10.1021/la030090w

Verbruggen B, Tóth T, Atalay YT et al (2013) Design of a flow-controlled asymmetric droplet splitter using computational fluid dynamics. Microfluid Nanofluidics 15:243–252. doi:10.1007/s10404-013-1139-3

Wang YZ, Zhao Y, Cho SK (2007) In-droplet magnetic beads concentration and separation for digital microfluidics. In: Solid-state sensors, actuators microsystems conference. TRANSDUCERS 2007. International. IEEE, pp 711–714

Warnke KC (2003) Finite-element modeling of the separation of magnetic microparticles in fluid. IEEE Trans Magn 39:1771–1777. doi:10.1109/TMAG.2003.810609

Whitesides GMG (2006) The origins and the future of microfluidics. Nature 442:368–373. doi:10.1038/nature05058

Whitesides GMG (2011) What comes next? Lab Chip 11:191–193. doi:10.1039/c0lc90101f

Zborowski M, Sun L, Moore LR et al (1999) Continuous cell separation using novel magnetic quadrupole flow sorter. J Magn Magn Mater 194:224–230. doi:10.1016/S0304-8853(98)00581-2